Spatial phase dislocations in femtosecond laser pulses

Kaloyan Bezuhanov and Alexander Dreischuh

Department of Quantum Electronics, Sofia University, 5, James Bourchier Boulevard, BG-1164 Sofia, Bulgaria

Gerhard G. Paulus

Max-Planck-Institut für Quantenoptik, Hans-Kopfermann-Strasse 1, D-85748 Garching, Germany, Sektion Physik, Ludwig-Maximillians-Universität, Am Coulombwall 1, D-85747 Garching, Germany, and Department of Physics, Texas A&M University, College Station, Texas 77843-4242

Michael G. Schätzel and Herbert Walther

Max-Planck-Institut für Quantenoptik, Hans-Kopfermann-Strasse 1, D-85748 Garching, Germany, and Sektion Physik, Ludwig-Maximillians-Universität, Am Coulombwall 1, D-85747 Garching, Germany

Dragomir Neshev, Wieslaw Królikowski, and Yuri Kivshar

Nonlinear Physics Centre and Laser Physics Centre, Research School of Physical Sciences and Engineering, Australian National University, Canberra ACT 0200, Australia

Received March 1, 2005; revised July 11, 2005; accepted July 12, 2005

We show that spatial phase dislocations associated with optical vortices can be embedded in femtosecond laser beams by computer-generated holograms, provided that they are built in a setup compensating for the introduced spatial dispersion of the broad spectrum. We present analytical results describing two possible arrangements: a dispersionless 4***f*** setup and a double-pass grating compressor. Experimental results on the generation of optical vortices in the output beam of a 20 fs Ti:sapphire laser and the proof-of-principle measurements with a broadband-tunable cw Ti:sapphire laser confirm our theoretical predictions. © 2006 Optical Society of America

OCIS codes: 050.1970, 090.1760, 120.5060, 140.3300, 140.7090.

1. INTRODUCTION

The presence of phase dislocations in the wavefront of a light beam determines its phase and intensity structure. Since the phase becomes indeterminate at the singularity point, both the real and the imaginary parts of the field amplitude (i.e., also the field intensity) vanish.[1] Each one-dimensional (1D) π-phase dislocation is coupled with a zero-intensity line [one-dimensional odd dark beam (1D ODB)]. An isolated point singularity with a screw-type phase distribution is associated with an optical vortex (OV). The characteristic helical phase profiles of OVs are described by $\exp(im\theta)$ multipliers, where θ is the azimuthal coordinate and the integer number m is their topological charge. As shown in Ref. 2, an m-fold-charged OV beam carries an orbital angular momentum of $m\hbar$ per photon, independent of the spin angular momentum (i.e., on the polarization state). Recently, free-space transfer of information encoded as orbital angular momentum was demonstrated,[3] in which the inherent security of the data depended on topological rather than on mathematical encryption.

The understanding of the linear spatiotemporal behavior of focused femtosecond beams with phase singularities is of both theoretical and experimental interest. Remarkable spectral changes take place in the neighborhood of phase singularities near the focus of a converging, spatially fully coherent polychromatic wave.[4] Broadband illumination leads to nonnegligible chromatic effects in the vortex region even in the case of compensated spectral dispersion.[5,6]

In self-defocusing media the nonlinearity is able to compensate for the dark-beam diffraction, and dark spatial solitons have been generated[7–9] in a variety of materials. In self-focusing media, OV beams are unstable,[10] except for the case of partial incoherence[11] or nonlocal nonlinear response or both.[12,13] Instability-induced breakup of OVs to a controllable number of bright spatial solitons has lead to the concepts of soliton molecules[14] and soliton algebra.[15–19] All types of soliton application will benefit from ultrashort pulses carrying spatial phase dislocations, since such pulses exhibit peak intensities high enough to access optical nonlinearities in many materials. These concepts, along with the difficulties associated with the generation of subpicosecond helical (spinning) solitons in optical fibers[20] and stable spinning optical solitons in three dimensions,[21] indicate the importance of the problem. Phase dislocations in femtosecond laser fields may also provide a new degree of freedom in experiments such as phase-controlled high-harmonic generation.

0740-3224/06/010026-10/$15.00

The challenge in creating spatial phase dislocations in short pulses with broad spectral bandwidths is to impose the desired dislocation onto all spectral components while keeping the pulse width and shape undistorted[22] and the pulse front untilted. The known methods for generating phase singularities applicable in the cw and quasi-cw regimes are not suited for femtosecond lasers. Astigmatic transverse-mode converters[23,24] cannot be used directly, since they require transverse modes higher than the fundamental TEM_{00}. The approach[25] of preparing a Hermite–Gaussian-like (HG_{01}) mode at the entrance of the converter by splitting a HG_{00} mode and spatially offsetting its two out-of-phase halves seems feasible, but for femtosecond pulses it requires an additional interferometrically controlled delay line. Intracavity phase elements[26] and beam rotators[27,28] are not applicable in the femtosecond regime because of the emitted transverse mode. Transparent spiral wave plates[29,30] are less flexible in controlling the phase distribution dynamically as compared with liquid-crystal modulators structured in pie slices.[31,32] They all preserve the beam path, and the latter exhibits a high efficiency in energy conversion, in addition. In both cases, however, the magnitude of the phase jump of the dislocation will deviate from π for the different spectral components of the short pulse, and topological dispersion will be present.[33] Glass platelets of a varying thickness providing linear phase retardation on one half of a (cw) laser beam are able to produce OVs.[34] Because of the space-dependent dispersion and time delays, this technique cannot be applied to ultrashort pulses either.

A well-known[35] and widely used method to generate spatial phase dislocations is the reconstruction of computer-generated holograms (CGHs). This method can be used to realize screw,[36,37] step,[38,39] and mixed-type dislocations[40] as well as arrays of such dislocations[41] in first-order diffracted beams. To impose the encoded phase dislocation onto all spectral components of the ultrashort pulse while keeping the pulse undistorted, one must align the CGH as a part of an optical system with compensated spatial dispersion. We demonstrated recently[42] that a dispersionless 4***f*** system[43–45] provides one possible solution of the problem. Here we discuss in detail the application of a 4***f*** system for encoding phase defects in femtosecond laser pulses. Although our approach is well suited for femtosecond oscillators, schemes involving (chirped pulse) amplifiers would be troubled by the restless behavior of the dislocations, and amplified spontaneous emission in the dark core of the beam has to be expected. In the second part of this paper we show that the spatial dislocation can be efficiently encoded in an amplified femtosecond pulse by using a CGH in a double-pass grating-pair compressor.[46,47]

2. THEORETICAL MODEL

Without loss of generality, we normalize the electric field amplitude to unity and assume that the spatial profile of the optical field is Gaussian $E \sim \exp[-(x_0^2+y_0^2)/\sigma_0^2]$, where σ_0 is the beam width at the $1/e$ level and the aperture of the CGH is large enough not to cause edge diffraction. The field evolution after passing the CGH is analyzed by using the Fresnel integral

$$E(x,y,z=s) = \frac{\exp(iks)}{i\lambda s} \int\int E(x_0,y_0,0)\exp\left(\frac{i\pi r^2}{\lambda s}\right)\mathrm{d}x_0\mathrm{d}y_0. \tag{1}$$

Directly behind the CGH, it has the form

$$E(x_0,y_0,0) = T(x_0,y_0)\exp[-(x_0^2+y_0^2)/\sigma_0^2]. \tag{2}$$

In the above expressions $r^2=(x-x_0)^2+(y-y_0)^2$, λ is a particular wavelength within the generated spectral bandwidth, $k=2\pi/\lambda$, and $T(x_0,y_0)$ is the grating transmission function containing the phase profile $\varphi(x_0,y_0)$ of the desired dislocation. This function can be expanded in a Fourier series in terms of field amplitudes C_n of the different diffraction orders n:

$$T(x_0,y_0) = \sum_{n=-\infty}^{\infty} C_n \exp[in2\pi(x_0/d)]\exp[in\varphi(x_0,y_0)]. \tag{3}$$

Here d is the period of the diffraction grating imprinted on the CGH. In the particular case of a plane phase profile $\varphi(x_0,y_0)=\varphi_0$=constant, Eq. (3) describes the transmission of a diffraction grating with stripes perpendicular to the Ox_0 axis (see Fig. 1). The quantity $d\varphi_0/(2\pi)$ corresponds to the offset of the central transmitting stripe from the center of the coordinate system Ox_0y_0. The coefficients C_n depend on the particular profile of the stripes. For a binary CGH of perfectly transmitting and reflecting stripes of equal widths, $C_n=\sin(n\pi/2)/(n\pi)$.[48]

When a plane-wave reference beam is used for the generation of the hologram, the curvature of the CGH stripes decreases with increasing distance to the singularity, and the stripes appear perpendicular to the coordinate axis Ox_0, independent of the type of the encoded dislocation. Since we are interested in the ±1st diffracted order beams only, which reconstruct the encoded phase profile, we will analyze the electric field distribution at distances at which the diffracted orders are well separated.

3. CREATION OF PHASE DISLOCATIONS BY A SINGLE COMPUTER-GENERATED HOLOGRAM

The structure of the CGH for generating a 1D ODB and the coordinate system assigned to it are shown in Fig. 1.

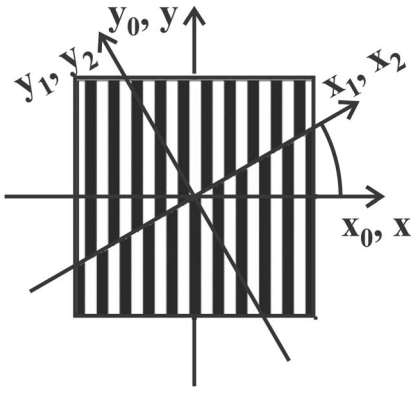

Fig. 1. CGH for generating a 1D ODB in a general (nonperpendicular) orientation of the dislocation axis with respect to the grating stripes.

In the general situation of a nonparallel orientation of the dislocation axis with respect to one of the coordinate system axes, the dislocation position is given by the straight-line equation $y=x\tan\alpha$. The encoded π-phase jump causes an offset of the stripes by half a period on both sides of the dislocation. This CGH (Fig. 1) can be considered to be composed of two identical half-gratings that are shifted with respect to each other. Let us assume that the grating is illuminated by a laser beam aligned in a way that the 1D dislocation crosses its center. Then the CGH transmission function can be written in the form

$$T_{\pm}(x_0,y_0) = C_1 \exp\left(i\frac{2\pi x_0}{d}\right)\exp\{i[\varphi_0 + \mathrm{sgn}(y_0 - x_0\tan\alpha)\pi/2]\}, \tag{4}$$

where the subscript ± refers to the value of the signum function, i.e., to the upper or lower half of the grating. The field just behind the grating is therefore given by

$$E'_{\pm}(x_0,y_0) = T_{\pm}(x_0,y_0)\exp[-(x_0^2+y_0^2)/\sigma_0^2]. \tag{5}$$

It is more convenient to evaluate the diffraction integral Eq. (1) in a coordinate system Ox_1,y_1 with the x_1 axis parallel to the 1D dislocation. After rotating the coordinate system by an angle α, we find that Eq. (5) becomes

$$E'_{y_1>0}(x_1,y_1) = \exp[-(x_1^2+y_1^2)/\sigma_0^2]T_{y_1>0}(x_1,y_1),$$

$$E'_{y_1<0}(x_1,y_1) = \exp[-(x_1^2+y_1^2)/\sigma_0^2]T_{y_1<0}(x_1,y_1). \tag{6}$$

Following the beam propagation in a coordinate system Ox_2y_2 parallel to Ox_1y_1 but located at a distance $z=s$, one can describe the electric field amplitude of the diffracted wave $E(x_2,y_2)$ by a sum of two integrals:

$$E(x_2,y_2) = \frac{\exp(iks)}{i\lambda s}\left[\int_{-\infty}^{\infty}\int_{0}^{\infty} E'_{y_1>0}(x_1,y_1)\exp\left(i\frac{\pi r_{21}^2}{\lambda s}\right) + \int_{-\infty}^{\infty}\int_{-\infty}^{0} E'_{y_1<0}(x_1,y_1)\exp\left(i\frac{\pi r_{21}^2}{\lambda s}\right)\right]dx_1dy_1, \tag{7}$$

where $r_{21}^2=(x_2-x_1)^2+(y_2-y_1)^2$. With the substitution $y_1\rightarrow -y_1$, denoting $r_i^2=x_i^2+y_i^2, i=1,2$, and after some routine mathematics, we can write the integrals as

$$E(x_2,y_2) = \frac{2C_1}{i\lambda s}\exp(i\varphi_0)\exp(iks)\exp\left(i\frac{\pi r_2^2}{\lambda s}\right) \times\int_{-\infty}^{\infty}\int_{0}^{\infty}\exp\left(-\frac{r_1^2}{\sigma_0^2}\right)\exp\left(i\frac{\pi r_1^2}{\lambda s}\right) \times\exp\left[-ikx_1\left(x_2-\frac{\lambda s}{d}\cos\alpha\right)\right] \times\sin\left[\frac{k}{s}y_1\left(y_2+\frac{\lambda s}{d}\sin\alpha\right)\right]dx_1dy_1. \tag{8}$$

The equation describing the position of the dislocation $y_2+(\lambda s/d)\sin\alpha=0$ arises from the physical requirement of a zero value of the electric field amplitude $E(x_2,y_2)$ for the diffracted wave at the position of the phase dislocation. In a coordinate system (x,y) with axes parallel to the initial (x_0,y_0) axes (see Fig. 1), the orientation of the dislocation at arbitrary $z=s$ is described by the condition

$$y = (x-\lambda s/d)\tan\alpha. \tag{9}$$

Hence, in the course of its propagation, the dislocation remains parallel to the one encoded in the CGH. However, there is a wavelength-dependent spatial offset (spatial dispersion) proportional to $\lambda s/d$. For a broadband illumination of the CGH, the only initial orientation of the 1D dislocation for which the integral intensity remains zero along the dislocation is the one encoded perpendicular to the CGH stripes, i.e., at an angle $\alpha=0$. This is intuitive because the spatial dispersion is perpendicular to the CGH stripes. Unfortunately, spatial chirp is inevitable. Its presence can be clearly recognized in Fig. 2 by the horizontal elongation of the beam.

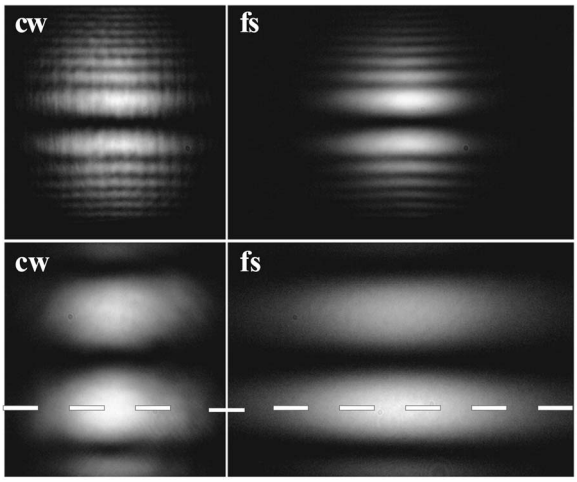

Fig. 2. Gray-scale images of the 1D ODB 17 (top) and 35 cm (bottom) behind a single CGH, for cw (left) and femtosecond (fs) laser beams (right). The dashed horizontal line marks the position where the cross section of the light intensity distributions has been taken (see Fig. 4).

The gray-scale images of the 1D ODB in the cw and femtosecond regimes are obtained by changing the operation regime of a Ti:sapphire laser. The oscillator is pumped by an intracavity-doubled $Nd:YVO_4$ (Millenia Vi) laser and emits nearly transform-limited 20 fs pulses at a repetition rate of 78 MHz with an average power of 200 mW at a central wavelength of 797 nm.[49] The eventual mode hopping of the femtosecond oscillator in cw[50] (lasing in one longitudinal mode at a time and hopping among different modes at nearly constant output power) will result in a spectral averaging during the camera acquisition and, as a consequence, could reduce the contrast of the experimental frames. In the measurements presented in the first part of this paper, binary CGHs produced photolithographically with a stripe period of $d=30$ μm are used, and the experimental frames are recorded with a CCD camera with 12 μm resolution. With the relatively low-resolution holograms used in this paper, the above-mentioned negative effect remains negligible. To demonstrate the influence of the beam diffraction, we show in the left column of Fig. 2 frames of 1D ODBs in cw regime 17 and 35 cm behind the hologram. The images in the right column are re-

corded at the same distances when mode locking was turned on. In Fig. 3 vertical cross sections of the images shown in Fig. 2 are compared. In both regimes the integral intensity approaches the zero level at the phase dislocation encoded perpendicularly to the grating stripes. The beam broadening along the 1D dislocation due to the spatial dispersion is much stronger in the femtosecond regime as compared with the cw. This is clearly seen in Fig. 4 (left), in which we compare horizontal slices taken parallel to the dislocation in both regimes (see marker in Fig. 2). Numerical simulations obtained by solving the Fresnel integral [Eq. (1)] for $z=0.6L_D$ ($L_D=k\sigma_0^2/2$) are shown in Fig. 4 (right). The broadening along the dislocation increases with increasing propagation path length (Fig. 2).

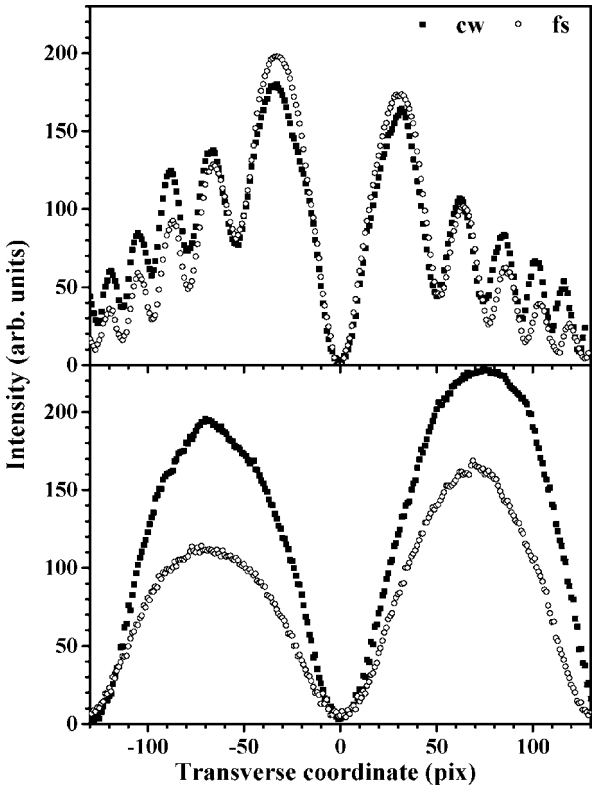

Fig. 3. Vertical cross sections of the images shown in Fig. 2. Solid squares, cw regime; open circles, femtosecond regime. Propagation distances are 17 (top) and 35 cm (bottom).

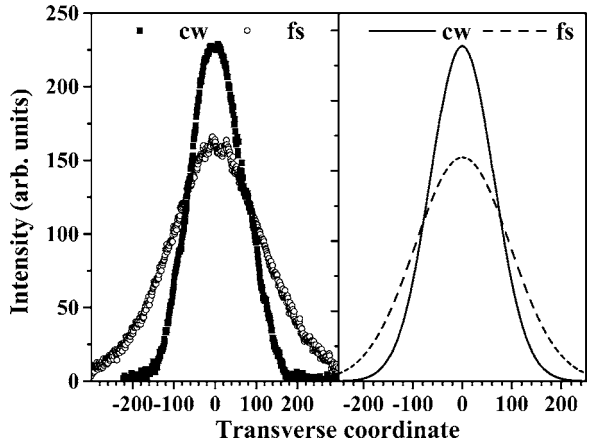

Fig. 4. Left graph: cross sections of the bottom images in Fig. 2 taken parallel to the 1D ODB. Right: numerical results for a propagation distance $z=0.6L_D$. Solid squares and solid curve, cw regime; open circles and dashed curve, femtosecond regime. The transverse coordinate is in CCD-camera pixels for the experimental profiles and in arbitrary units for the numerical ones.

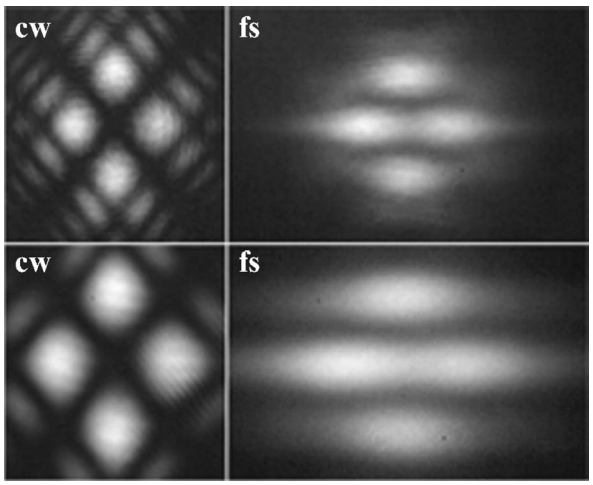

Fig. 5. Gray-scale images of a quasi-2D dark beam formed by crossed 1D phase dislocations, for cw and femtosecond laser beams. Top, 17 cm behind a single CGH; bottom, 35 cm behind.

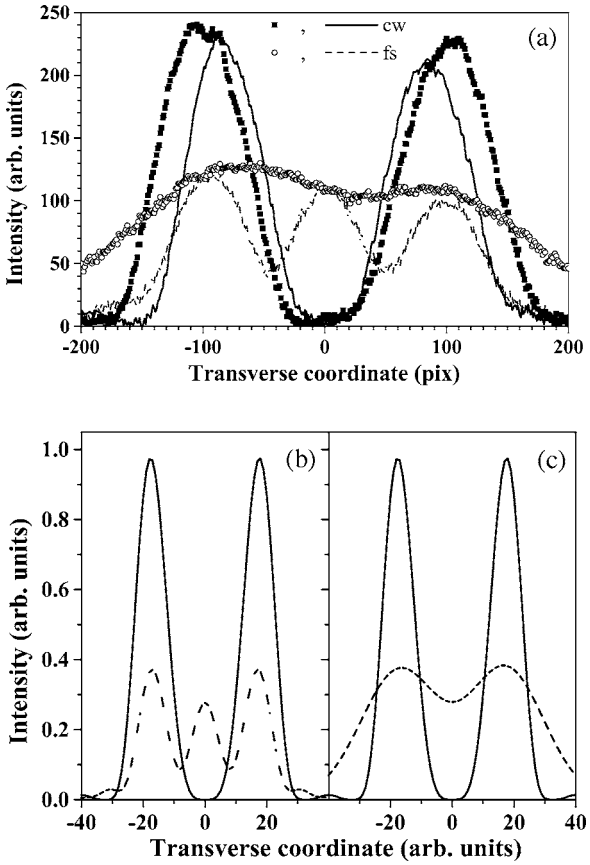

Fig. 6. (**a**) Central cross sections of the images shown in Fig. 5 for $z=35$ cm. Solid squares and solid curve, cw regime (horizontal and vertical slices, respectively); open circles and dashed curve, femtosecond regime (horizontal and vertical slices, respectively). (**b**) Numerically obtained vertical cross sections for propagation distance $z=0.6L_D$. Solid curve, cw regime; dashed curve, femtosecond regime. (**c**) The same as in (**b**) but in the horizontal direction.

For an arbitrary orientation of the 1D dislocation the integral intensity cannot be zero, since the position of the dislocation in each monochromatic spectral component depends on λ. A pair of perpendicular 1D phase dislocations was encoded in another CGH at an dislocation-to-stripe angle $\alpha=45$ deg. The results observed in the cw and femtosecond regimes are shown in Fig. 5 for the same propagation distances (17 and 35 cm) after the CGH. Figure 6(a) is aimed to accentuate (solid squares and solid curve depict horizontal and vertical slices, respectively) that, similar to the 1D case, the cw quasi-2D dark beam retains its high contrast. Owing to the spatial dispersion of the CGH, the dislocations generated in the different spectral components in the femtosecond regime are displaced, and the intensity modulation degenerates (in Fig. 6(a), open circles and dashed curve depict horizontal and vertical slices, respectively). The cross sections extracted from the bottom images shown in Fig. 5 agree qualitatively well with the numerical profiles presented in Figs. 6(b) and 6(c). At large propagation distances the uncompensated dispersion in the femtosecond regime results in the formation of horizontal gray stripes (see Fig. 5) instead of a black cross.

4. TWO-DIMENSIONAL DISLOCATION AND ANALYSIS OF THE 4*f* SYSTEM

The optical vortex (OV) is an object localized in two transverse dimensions. When generated by a single CGH, the spatial dispersion displaces the vortices in the individual spectral components. This can clearly be seen in Fig. 7, in which we show gray-scale images of OV beams recorded at two distances behind a CGH, in both the cw and the femtosecond regimes. The contrast of the broadband OV is gradually reduced as compared with that of the monochromatic beam under comparable conditions (Fig. 7, left graph: $z=35$ cm). This behavior is confirmed by numerical simulation shown in Fig. 7 (right graph).

In the expansion of the grating transmission function $T(x_0,y_0)$ [Eq. (3)], the multiplier accounting for the angular dispersion $\exp(i2\pi n x_0/d)$ does not depend on the particular form of the encoded phase profile $\varphi(x_0,y_0)$. This allows one to compensate for the dispersion introduced by the CGH by using a suitable optical system involving an additional grating with the same period d without any influence on the phase distribution $\varphi(x_0,y_0)$. This requirement is satisfied by a dispersionless 4***f*** system[43–45] as shown in Fig. 8.

To obtain the evolution of the electric field inside the 4f setup (Fig. 8), we use the integral relation between the field distributions in the front and back focal planes of a thin lens,

$$E(x_f,y_f)=\frac{1}{\lambda f}\int\int E_0\exp\left[-i\frac{k}{f}(x_0x_f+y_0y_f)\right]\mathrm{d}x_0\mathrm{d}y_0, \tag{10}$$

which is obtained from the diffraction integral [Eq. (1)] accounting for the transmission

$$t(x,y)=\exp(iknd_0)\exp\left[-i\frac{k}{2f}(x^2+y^2)\right] \tag{11}$$

of the thin lens of optical thickness nd_0 and focal length ***f***. For simplicity, the constant phase multipliers and the

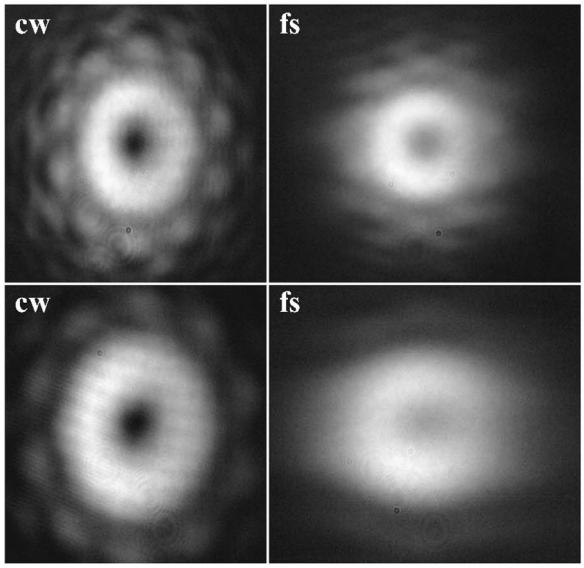

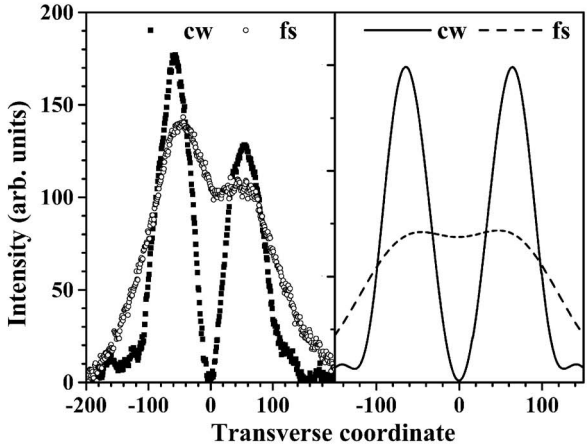

Fig. 7. Gray-scale images of OV beams 17 (top) and 35 cm (bottom) behind a single CGH, for cw and femtosecond laser beams. Graph: corresponding horizontal cross sections of the OV beams recorded at 35 cm (left) and numerical results for propagation distance $0.6L_D$ (right). The transverse coordinate is in CCD-camera pixels for the experimental profiles and in arbitrary units for the numerical ones.

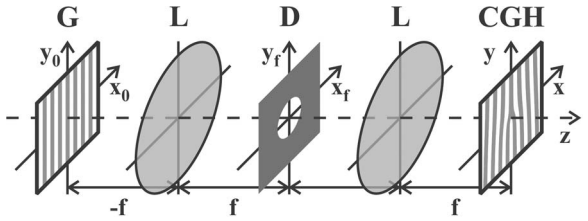

Fig. 8. Illustration of the 4***f*** setup that is analyzed theoretically. G, diffraction grating; CGH, computer-generated hologram with an encoded phase singularity; L, lenses of focal length ***f***; D, iris diaphragm. The input, Fourier, and output planes are denoted by indices 0, ***f***, and 1, respectively.

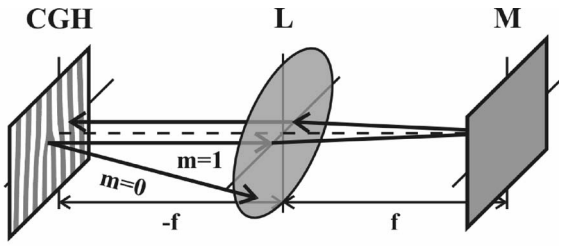

Fig. 9. Illustration of the folded 4*f* setup that is used in the experiment. CGH, computer-generated hologram; L, quartz lens; M, silver-coated mirror.

quadratic phase terms introduced by the lenses are omitted. The lens apertures are considered to be much larger as compared with the spatial extent of the beam at the respective planes. In the particular case of an incoming Gaussian background beam, the first-order diffracted wave just after the first grating G (see Fig. 8) is given by

$$E'(x_0,y_0) = C_1 \exp\left(-\frac{x_0^2+y_0^2}{\sigma_0^2}\right)\exp\left(i\frac{2\pi}{d}x_0\right), \qquad (12)$$

and its distribution $E(x_f,y_f)$ in the back focal plane of the first lens is

$$E(x_f,y_f) = \frac{\sigma_0^2}{\pi\lambda f}C_1 \exp\left[-\frac{\left(x_f-\frac{\lambda f}{d}\right)^2+y_f^2}{\left(\frac{\lambda f}{\pi\sigma_0}\right)^2}\right]. \qquad (13)$$

The analysis of 4*f*-type systems has been the subject of extensive research in connection with their wide application in pulse-shaping experiments.[43–45] Here the iris diaphragm does not affect the propagation of the first-order diffracted beam passing through the 4*f* system and removes all other diffracted order beams only. Applying again the transformation [Eq. (10)], one gets the field distribution in front of the CGH:

$$E(x,y) = \frac{C_1}{\lambda^2 f^2}\exp\left[-\frac{x^2+y^2}{(\beta\sigma_0)^2}\right]\exp\left(i\frac{2\pi}{\beta d}x\right), \qquad (14)$$

where β is the angular magnification of the optical system. The transmission function of the first-order diffracted beam is given by $T(x,y)=A_1\exp(i2\pi x/d)\times\exp[i\varphi(x,y)]$.[48] In this way we derive an analytical expression for the electric field amplitude $E'(x,y)$ at the exit of the 4*f* system:

$$E'(x,y) = \frac{C_1A_1}{(\pi\lambda f)^2}\exp\left[-\frac{x^2+y^2}{(\beta\sigma_0)^2}\right]\exp[i\varphi(x,y)] \times\exp\left[i\frac{2\pi}{d}\left(1+\frac{1}{\beta}\right)x\right]. \qquad (15)$$

The last multiplier in Eq. (15) accounts for the net spatial dispersion at the exit. For a perfect alignment, $\beta=-1$, and the 4*f* system is dispersion free. Therefore, arbitrary-oriented dark beams with phase dislocations generated in each individual spectral component are recombined spatially and temporally to overlap at the exit without any chirp.

The 4*f* setup used in our experiment (Fig. 9) is folded in the Fourier plane by a silver-coated mirror. A large-aperture (2.5 cm) quartz lens with a focal length $f=20$ cm is aligned carefully to minimize aberrations. A binary CGH of an OV is positioned in a way to reconstruct the encoded point phase dislocation in the center of the background beam. In the peripheral part of this grating the stripes are parallel. This region is used as an effective second grating to recombine the spectral components at the exit. In Fig. 10 (top figures) gray-scale images of OVs recorded 35 cm after the exit of the 4*f* setup are shown. The frames are taken in the cw and femtosecond regimes successively by our turning the mode locking on and off while keeping the alignment unchanged. Interference lines in the frame in Fig. 10 recorded for cw can clearly be seen. They appear owing to slight overlapping of the OV beam exiting the 4*f* system with a beam reflected directly from the CHG substrate. Owing to the lack of temporal overlapping and the reduction of the coherence length, both interference and speckles disappear in the femtosecond regime. In comparison with the lower right frame in Fig. 7, the contrast of the femtosecond OV shown in Fig. 10, right frame, is clearly improved and can be maximized by one's filtering out all parasitic reflections. An estimation based on the visibility of the interference structure in the cw regime (Fig. 10, left frame) shows a $(10\pm3)\%$ contribution of such reflections to the background signal in the vortex core. The influence of these reflections in the femtosecond regime is likely to be stronger, since the directly reflected broadband signal is actually dispersed in space. The graph in Fig. 10 shows vertical cross sections of the cw and femtosecond OV beams (solid squares and

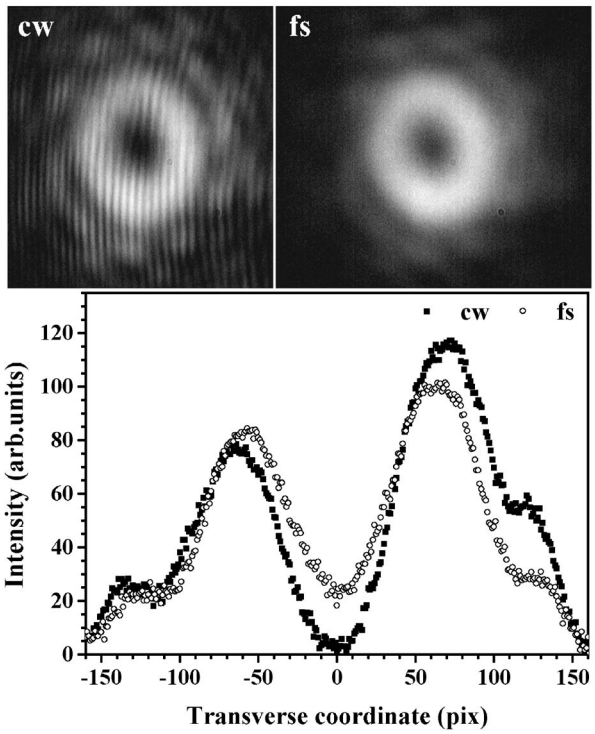

Fig. 10. Frames: OVs recorded 35 cm after the 4*f* setup in the cw and the femtosecond regimes. Graph: corresponding vertical cross sections of OV beams in the cw and femtosecond regimes (solid squares and open circles, respectively).

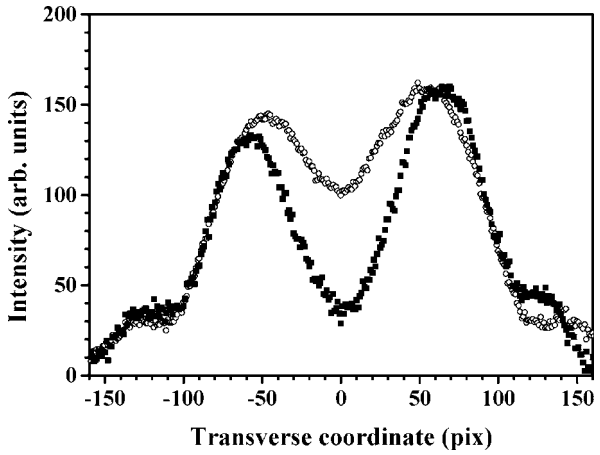

Fig. 11. Comparison between the OV cross sections taken parallel to the stripes of the CGH in the femtosecond regime. Open circles, single CGH; solid squares, folded 4***f*** setup.

open circles, respectively). The improvement of the contrast in the OV beam core is once again confirmed (see Fig. 11) by our comparing the beam profiles for the cases in which a single CGH and a CGH in a 4***f*** system are used.

As long as no pulse shaping is to be performed in the Fourier plane, the low-resolution $d\lambda/dx_f = 150$ nm/mm related to the 30 μm grating period is acceptable. Temporal pulse shaping in the same 4***f*** system would require much denser gratings and lenses and focusing mirrors of shorter focal lengths.

5. CREATION OF PHASE DISLOCATIONS IN THE PULSE COMPRESSION PROCESS

In the following we will demonstrate that dark beams carrying phase dislocations can be generated in double-pass grating compressors[46,47] without introducing additional spatial dispersion. One of the gratings (in this theoretical model, the last one) has to be replaced by a CGH of a period d equal to that of the other grating(s). The optical scheme analyzed is shown in Fig. 12.

Theoretical analysis of this system amounts to evaluation of the diffraction integral between the planes in which the diffraction gratings are located. To calculate the field distribution in the plane (x_2,y_2) of the second grating, we shift the input plane (x_0,y_0) at a distance $z = s_0$ in front of it. (This shift is arbitrary and can later be set equal to zero.) Omitting the constant phase multipliers, we can describe the transmission functions of each grating and the CGH as follows:

$$T(x_1,y_1) = C_1 \exp[i(2\pi/d)x_1],$$

$$T(x_j,y_j) = C_1 \exp[-i(2\pi/d)x_j], \quad j = 2,3,$$

$$T(x,y) = C_1 \exp[i(2\pi/d)x]\exp[\varphi(x,y)]. \tag{16}$$

A plus or minus sign in the phase corresponds to beam propagation in the first or in the minus first diffraction order of the respective grating. One can obtain the electric field distribution $E'(x_2,y_2)$ just after the second grating by multiplying the field diffracted between the (x_1,y_1) and (x_2,y_2) planes by the transmission function $T(x_2,y_2)$. The field distribution needed to evaluate the diffraction integral is a product of the field diffracted between the (x_0,y_0) and (x_1,y_1) planes and the transmission function $T(x_1,y_1)$ of the first grating. Therefore,

$$\begin{aligned} E'(x_2,y_2) = {} & \frac{-C_1}{\lambda^2 s_0 l}\exp\left(-i\frac{2\pi x_2}{d}\right)\exp[ik(s_0+l)] \\ & \times \int\int \left[C_1 \exp\left(i\frac{2\pi x_1}{d}\right) \right. \\ & \left. \times \int\int E(x_0,y_0)\exp\left(i\frac{\pi r_{10}^2}{\lambda s_0}\right)dx_0 dy_0 \right] \\ & \times \exp\left(i\frac{\pi r_{21}^2}{\lambda l}\right)dx_1 dy_1, \end{aligned} \tag{17}$$

where $r_{ij}^2 = (x_i - x_j)^2 + (y_i - y_j)^2, i,j = 0, 1, 2$. Changing the order of integration and integrating over x_1 and y_1, we find that the field after the first pass through the compressor (i.e., after the second grating; see Fig. 12) is

$$\begin{aligned} E' = (x_2,y_2) = {} & \frac{C_1^2}{i\lambda(s_0+l)}\exp[ik(s_0+l)]\exp\left[-i\frac{\pi s_0 l\lambda}{(s_0+l)d^2}\right] \\ & \times \int\int E(x_0,y_0) \\ & \times \exp\left[-i\frac{2\pi l(x_2-x_0)}{(s_0+l)d}\right] \\ & \times \exp\left[i\frac{\pi r_{20}^2}{\lambda(s_0+l)}\right]dx_0 dy_0. \end{aligned} \tag{18}$$

The evolution of the optical field amplitude during the second pass through the compressor—i.e., between the (x_2,y_2) plane and the output (x,y) plane—is modeled in the same way. Since the output grating of the compressor is chosen to be the CGH, the output electric field amplitude $E'(x,y)$ contains the phase multiplier $\varphi(x,y)$. After some algebra we get

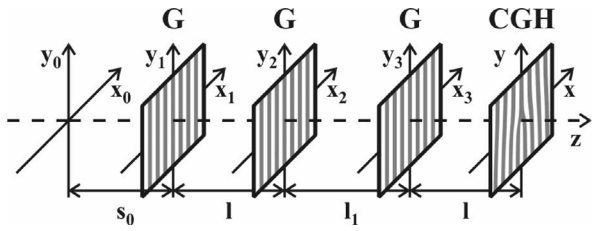

Fig. 12. Illustration of the double-pass grating compressor that is analyzed theoretically. G, diffraction gratings; CGH, computer-generated hologram with an encoded phase singularity; l, compressor length. The planes of the gratings are indexed successively. The CGH is assumed to stand at the exit of the compressor.

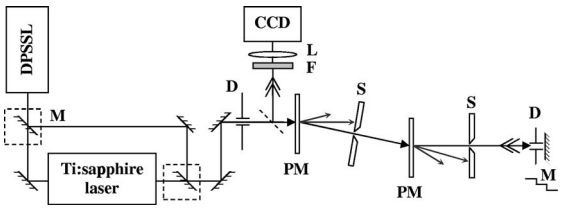

Fig. 13. Setup of the proof-of-principle experiment. PM, phase masks (phase CGHs); D, iris diaphragm; S, slit; M, removable mirrors (dashed boxes) and folding mirror ensuring vertical offset in the reverse pass through the system; F, filter; L, imaging lens (f=2 cm); DPSSL, diode-pumped solid-state laser (Verdi V5); CCD, charge-coupled device camera.

$$E'=(x,y)=\frac{C_1^2}{i\lambda(l_1+l)}\exp[ik(l_1+l)]\exp[\varphi(x,y)]\times\exp\left[-i\frac{\pi l_1 l\lambda}{(l_1+l)d^2}\right]\times\int\int E'(x_2,y_2)\exp\left[-i\frac{2\pi l(x-x_2)}{d(l_1+l)}\right]\times\exp\left[i\frac{\pi r^2}{\lambda(l_1+l)}\right]dx_2dy_2, \quad (19)$$

where $r^2=(x-x_2)^2+(y-y_2)^2$. After substituting Eq. (18) in to Eq. (19) and integrating over x_2 and y_2, we can write the output amplitude of the electric field in a compact form:

$$E(x,y)=C_1^4E_{\text{diff}}\exp\{ik[s-l(\lambda/d)^2]\}\exp[\varphi(x,y)]. \quad (20)$$

Here E_{diff} is the electric field amplitude diffracted in the course of the optical beam propagation in the compressor [accurate to accumulated linear phase $\exp(iks)$; see Eq. (1)]. The first phase term in Eq. (20) accounts for the different propagation path lengths (and transit times) of the different spectral components, i.e., for the negative group-velocity dispersion of the grating compressor. The last term contains the phase profile encoded in the CGH. Because of symmetry reasons, the same result holds when the dislocation is generated by the first grating.

In the following, the behavior of the phase dislocations carried by the broad bandwidth of femtosecond laser pulses is imitated by sets of measurements conducted with a cw laser tuned at different wavelengths. In that sense, but without loss of generality, the following experiment serves as a proof of principle. The setup of the grating compressor is shown in Fig. 13. It consists of two identical phase masks (PMs) of OV. The PMs are phase CGHs fabricated directly on photoresist with stripe periods of 80 μm. Their higher (30%) efficiencies in the first diffraction order and large apertures (of 1.2 cm) were important in this measurement. To avoid dispersion in two spatial dimensions, we prealigned the gratings under the microscope so the stripes are parallel. Then the compressor scheme is aligned with the 532 nm output of a diode-pumped solid-state laser (Verdi V5). After two mirrors have been removed (Fig. 13, dashed boxes) the same laser is used to pump a cw tunable Ti:sapphire ring laser (Coherent 899-21). The diffracted beams of corresponding order after each PM are transmitted by two slits during the first pass through the compressor. A plane silver-coated mirror is used to reflect the infrared beam back for the second pass. It intentionally introduces a small vertical angular tilt (along the grating stripes) that allows one to separate the output beam from the input one and to encode a phase singularity only once—at the entrance or at the exit of the setup—even using identical CGHs. The output is imaged by a quartz lens (f=20 cm) directly on the array of a CCD camera of 8 μm resolution. The PM-to-PM distances (25 to 58 cm) are chosen such that the individual diffraction orders can be separated. The PM-to-folding-mirror distance [limited by the half-aperture of the PMs (1.2 cm)] was chosen in the same range.

The positions of the 0th- and ±1 st-order beams diffracted by the PM at the exit of the compressor are plotted in Fig. 14 as a function of wavelength. The wavelengths are measured by a wavemeter (Burleigh, WA-1100). Since in this measurement an OV is embedded in the beam by the first PM, it passes through the entire system, and all three output beams carry OVs. This was done in order to use the OVs as spatial markers. Only one of the beams passes through the setup as would be required for a real double-pass grating compressor.[46,47] It can clearly be seen that the OV nested in this beam preserves its position in space. The straight line in Fig. 14 represents a wavelength-independent OV position accurate within a standard deviation of two CCD-camera pixels when the laser wavelength is tuned in a 80 nm broad spectral interval. In contrast, the positions of the zero-order and idler first-order beams (middle and upper curves, respectively) change monotonically.

Although ultrashort pulses have broad spectra and a fixed phase relation between the spectral components, we measure the spatial positions of the vortices at discrete wavelengths only. Therefore, the experiment can be thought of as being a proof of principle. Nevertheless, taking the real spectrum of an amplified ultrashort pulse[49] and integrating a set of laser-beam power-density distributions recorded experimentally at discrete wavelengths, one can simulate the encoding of phase dislocations in a real double-pass grating compressor. The gray-scale in-

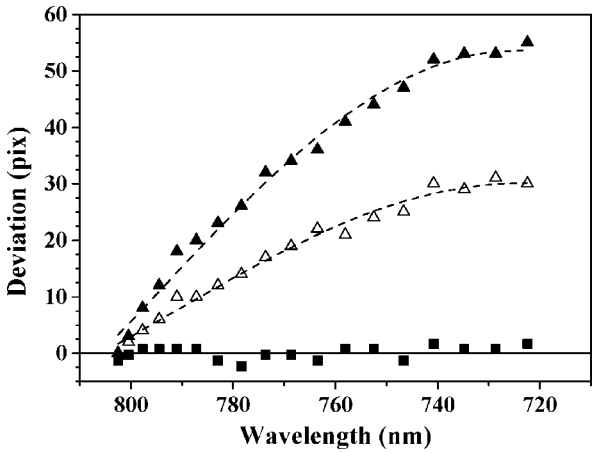

Fig. 14. Position of the OV at the exit plane of the pulse compressor as a function of the wavelength. Squares and triangles (solid and dashed curves) correspond to dispersion compensated and two uncompensated (zero-order and idler) beams, respectively. The dislocation is reproduced by the first PM.

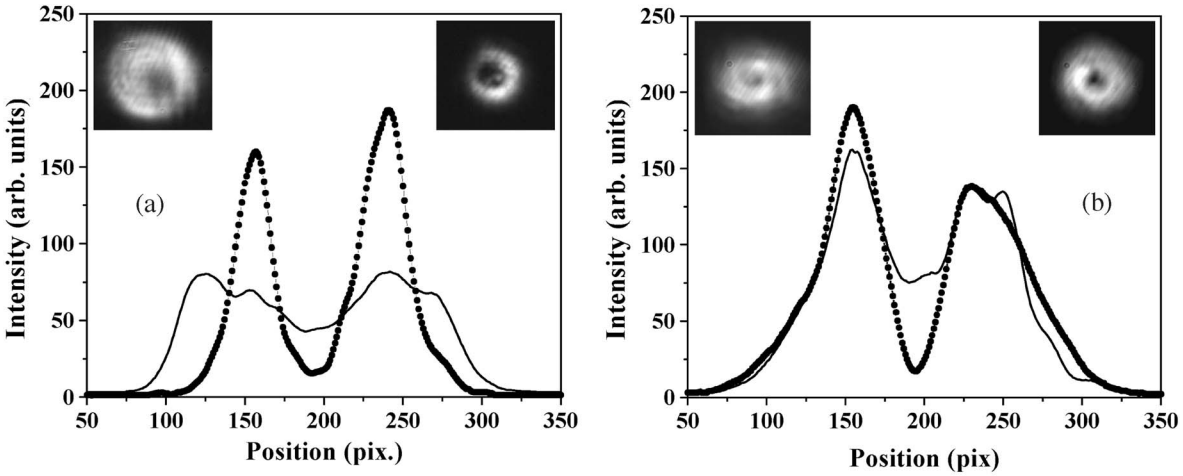

Fig. 15. Proof-of-principle simulations with OVs encoded in the (**a**) first and (**b**) last diffraction from a PM. Graphs: transverse cross sections of the uncompensated idler (solid curve) and desired OV (dotted curve). Insets: spectrally integrated experimental gray-scale images (idler, left; compensated OV, right).

sets in Figs. 15(a) and 15(b) are created in this way. Figure 15(a) refers to the 50 cm long compressor, in which the OV is encoded by the first PM. Because of diffraction, the spectrally integrated desired OV beam (right inset) is much broader as compared with the one exiting the longer setup (75 cm) where it was encoded by the last PM [Fig. 15(b), right inset]. The uncompensated spatial dispersion of the different spectral components in the modeled idler beam [Fig. 15(b), left inset] closely resembles the intensity distribution of an OV generated by a single CGH (Fig. 7, right images). The dotted and solid curves in Figs. 15(a) and 15(b) represent profiles of the compensated and idler output beams. The clearly higher contrast of the OV generated in the compressor as compared with the contrast of the idler vortex in both cases strongly supports the general conclusion of this analysis: Dark beams carrying phase dislocations can be generated in chirped femtosecond laser beams by using the respective holograms in a grating compressor scheme. Real adoption of this scheme in femtosecond systems requires ten-times-denser holographic diffraction gratings, which should not be a technical problem.

6. CONCLUSION

Our analytical and experimental results demonstrate the possibility of creating spatial phase dislocations in broadband (e.g., femtosecond) optical fields by using computer-generated holograms. In order to cancel the spatial dispersion introduced, these specifically designed diffraction gratings have to be implemented in 4***f*** setups or in double-pass grating compressors. The first approach does not affect the width of the ultrashort pulses and can be used directly with femtosecond oscillators. When (chirped pulse) amplifiers are involved in the femtosecond laser systems, the phase dislocations can be generated in all spectral components at the later stage of the pulse shortening in a grating compressor. In addition, our results are directly applicable to tunable laser beams when they have to preserve the positions of the spatial phase dislocations, as well as to encode phase dislocations in white-light-type beams.

ACKNOWLEDGMENTS

This research was partially supported by the National Science Fund (Bulgaria), under contract F-1303/2003, and the Australian Research Council. Corresponding author A. Dreischuh can be reached by e-mail at ald@phys.uni-sofia.bg.

REFERENCES

1. J. F. Nye and M. V. Berry, "Dislocations in wave trains," Proc. R. Soc. London Ser. A **336**, 190–191 (1974).
2. L. Allen, S. M. Barnett, and M. J. Padget, *Optical Angular Momentum* (Institute of Physics, 2004).
3. G. Gibson, J. Courtial, M. J. Padgett, M. Vasnetsov, A. Pas'ko, S. M. Barnett, and S. Franke-Arnold, "Free-space information transfer using light beams carrying orbotal angular momentum," Opt. Express **12**, 5448–5456 (2004).
4. G. Gbur, T. D. Visser, and E. Wolf, "Anomalous behavior of spectra near phase singularities of focused waves," Phys. Rev. Lett. **88**, 013901 (2002).
5. M. V. Berry, "Coloured phase singularities," New J. Phys. **4**, 66.1–66.14 (2002).
6. J. Leach and M. J. Padgett, "Observation of chromatic effects near a white-light vortex," New J. Phys. **5**, 154.1 (2003).
7. G. A. Swartzlander, Jr., D. R. Andersen, J. J. Regan, H. Yin, and A. E. Kaplan, "Spatial dark-soliton stripes and grids in self-defocusing materials," Phys. Rev. Lett. **66**, 1583–1586 (1991).
8. G. A. Swartzlander, Jr., and C. T. Law, "Optical vortex solitons observed in Kerr nonlinear media," Phys. Rev. Lett. **69**, 2503–2506 (1992).
9. Yu. S. Kivshar and G. P. Agrawal, *Optical Solitons* (Academic, 2003).
10. D. V. Skryabin and W. J. Firth, "Dynamics of self-trapped beams with phase dislocation in saturable Kerr and quadratic nonlinear media," Phys. Rev. E **58**, 3916–3930 (1998).
11. C.-C. Jeng, M.-F. Shih, K. Motzek, and Yu. S. Kivshar, "Partially incoherent optical vortices in self-focusing nonlinear media," Phys. Rev. Lett. **92**, 043904 (2004).
12. A. I. Yakimenko, Y. A. Zaliznyak, and Yu. S. Kivshar, "Stable vortex solitons in nonlocal self-focusing nonlinear media," http://lanl.arxiv.org/abs/nlin.PS/0411024.
13. D. Briedis, D. E. Petersen, D. Edmundson, W. Królikowski, and O. Bang, "Ring vortex solitons in nonlocal nonlinear media," Opt. Express **13**, 435–443 (2005), http://www.opticsexpress.org/abstract.cfm?URI=OPEX-13-2-435.

14. A. Desyatnikov, C. Denz, and Yu. S. Kivshar, "Nonlinear optical beams carrying phase dislocations," J. Opt. A **6**, S209–S212 (2004).
15. D. V. Petrov, L. Torner, J. Martorell, R. Vilaseca, J. P. Torres, and C. Cojocaru, "Observation of azimuthal modulational instability and formation of patterns of optical solitons in a quadratic nonlinear crystal," Opt. Lett. **23**, 1444–1446 (1998).
16. G. Molina-Terriza, J. Recolons, and L. Torner, "The curious arithmetic of optical vortices," Opt. Lett. **25**, 1135–1137 (2000).
17. I. Freund and A. Belenkiy, "Higher-order extrema in two-dimensional wave fields," J. Opt. Soc. Am. A **17**, 434–446 (2000).
18. L. Torner and A. P. Sukhorukov, "Quadratic solitons," Opt. Photonics News **13**, 42–47 (2002).
19. S. Minardi, G. Molina-Terriza, P. Di Trapani, J. P. Torres, and L. Torner, "Soliton algebra by vortex-beam splitting," Opt. Lett. **26**, 1004–1006 (2001).
20. B. A. Malomed, G. D. Peng, and P. L. Chu, "Helical versus fundamental solitons in optical fibers," Phys. Scr. **63**, 386–390 (2001).
21. D. Mihalache, D. Mazilu, L.-C. Crasovan, I. Towers, A. V. Buryak, B. A. Malomed, L. Torner, J. P. Torres, and F. Lederer, "Stable spinning optical solitons in three dimensions," Phys. Rev. Lett. **88**, 073902 (2002).
22. F. Grasbon, A. Dreischuh, F. Zacher, G. G. Paulus, and H. Walther, "Femtosecond interferometric autocorrelations in the presence of pulse front distortions," in *Tenth International School on Quantum Electronics: Laser Physics and Applications*, P. A. Atanasov and D. V. Stoyanov, eds., Proc. SPIE **3571**, 164–168 (1999).
23. M. W. Beijersbergen, L. Allen, H. E. L. O. van der Veen, and J. P. Woerdman, "Astigmatic laser mode converters and transfer of orbital angular momentum," Opt. Commun. **96**, 123–132 (1993).
24. M. J. Padgett and L. Allen, "Orbital angular momentum exchange in cylindrical-lens mode converters," J. Opt. B: Quantum Semiclassical Opt. **4**, S17–S19 (2002).
25. D. V. Petrov, F. Canal, and L. Torner, "A simple method to generate optical beams with a screw phase dislocation," Opt. Commun. **143**, 265–267 (1997).
26. R. Oron, N. Davidson, A. Friesem, and E. Hasman, "Efficient formation of pure helical laser beams," Opt. Commun. **182**, 205–208 (2000).
27. E. Abramochkin, N. Losevsky, and V. Volostnikov, "Generation of spiral-type laser beams," Opt. Commun. **141**, 59–64 (1997).
28. A. V. Smith and D. J. Armstrong, "Generation of vortex beams by an image-rotating optical parametric oscillator," Opt. Express **11**, 868–873 (2003), http://www.opticsexpress.org/abstract.cfm?URI=OPEX-11-8-868.
29. M. W. Beijersbergen, R. P. C. Coerwinkel, M. Kristensen, and J. P. Woerdman, "Helical-wavefront laser beams produced with a spiral phaseplate," Opt. Commun. **112**, 321–327 (1994).
30. A. G. Peele, P. J. McMahon, D. Paterson, Ch. Q. Tran, A. P. Mancuso, K. A. Nugent, J. P. Hayes, E. Harvey, B. Lai, and I. McNulty, "Observation of an x-ray vortex," Opt. Lett. **27**, 1752–1754 (2002).
31. D. Ganic, X. Gan, M. Gu, M. Hain, S. Somalingam, S. Stankovic, and T. Tschudi, "Generation of doughnut laser beams by use of a liquid-crystal cell with a conversion efficiency near 100%," Opt. Lett. **27**, 1351–1353 (2002).
32. Q. Wang, X. W. Sun, and P. Shum, "Generating doughnut-shaped beams with large charge numbers by use of liquid-crystal spiral phase plates," Appl. Opt. **43**, 2292–2297 (2004).
33. G. A. Swartzlander, Jr., and J. Schmit, "Temporal correlation vortices and topological dispersion," Phys. Rev. Lett. **93** 093901 (2004).
34. G.-H. Kim, J.-H. Jeon, K.-H. Ko, H.-J. Moon, J.-H. Lee, and J.-S. Chang, "Optical vortices produced with a nonspiral phase plate," Appl. Opt. **36**, 8614–8621 (1997).
35. N. R. Heckenberg, R. McDuff, C. P. Smith, and A. G. White, "Generation of optical phase singularities by computer-generated holograms," Opt. Lett. **17**, 221–223 (1992).
36. Z. S. Sacks, D. Rozas, and G. A. Swartzlander, Jr., "Holographic formation of optical-vortex filaments," J. Opt. Soc. Am. B **15**, 2226–2234 (1998).
37. A. Dreischuh, G. G. Paulus, F. Zacher, F. Grasbon, and H. Walther, "Generation of multiple-charged optical vortex solitons in a saturable nonlinear medium," Phys. Rev. E **60**, 6111–6117 (1999).
38. A. Dreischuh, G. G. Paulus, and F. Zacher, "Quasi-two-dimensional dark spatial solitons and generation of mixed phase dislocations," Appl. Phys. B **69**, 107–111 (1999).
39. A. Dreischuh, D. Neshev, G. G. Paulus, F. Grasbon, and H. Walther, "Ring dark solitary waves: experiment versus theory," Phys. Rev. E **66**, 066611 (2002).
40. A. Dreischuh, D. Neshev, G. G. Paulus, and H. Walther, "Experimental generation of steering odd dark beams of finite length," J. Opt. Soc. Am. B **17**, 2011–2017 (2000).
41. A. Dreischuh, S. Chervenkov, D. Neshev, G. G. Paulus, and H. Walther, "Generation of lattice structures of optical vortices," J. Opt. Soc. Am. B **19**, 550–556 (2002).
42. K. Bezuhanov, A. Dreischuh, G. G. Paulus, M. G. Schätzel, and H. Walther, "Vortices in femtosecond laser fields," Opt. Lett. **29**, 1942–1944 (2004).
43. A. M. Weiner, J. P. Heritage, and E. M. Kirschner, "High-resolution femtosecond pulse shaping," J. Opt. Soc. Am. B **5**, 1563–1572 (1988).
44. M. B. Danailov and I. P. Christov, "Time–space shaping of light pulses by Fourier optical processing," J. Mod. Opt. **36**, 725–731 (1989).
45. A. M. Weiner, "Femtosecond optical pulse shaping and processing," Prog. Quantum Electron. **19**, 161–237 (1995).
46. E. B. Treacy, "Compression of picosecond light pulses," Phys. Lett. **28** 34–35 (1968).
47. E. B. Treacy, "Optical pulse compression with diffraction gratings," IEEE J. Quantum Electron. **QE-5**, 454–458 (1969).
48. W.-H. Lee, "Computer generated holograms: techniques and applications" in *Progress in Optics*, E. Wolf, ed. (Elsevier North-Holland, 1978), Vol. 16.
49. F. Lindner, G. G. Paulus, F. Grasbon, A. Dreischuh, and H. Walther, "Dispersion control in a 100-kHz-repetition-rate 30-fs Ti:sapphire regenerative amplifier system," IEEE J. Quantum Electron. **38**, 1465–1470 (2002).
50. Y. Liu and P. Davis, "Synchronization of chaotic mode hopping," Opt. Lett. **25**, 475–477 (2000).